JOURNAL OF CATALYSIS 127, 645–664 (1991)

Non-Faradaic Electrochemical Modification of Catalytic Activity

III. The Case of Methanol Oxidation on Pt

C. G. VAYENAS* AND S. NEOPHYTIDES

Institute of Chemical Engineering and High Temperature Chemical Processes, Department of Chemical Engineering, University of Patras, Patras 26110, Greece

Received July 12, 1989; revised September 5, 1990

It was found that the catalytic activity and selectivity of polycrystalline Pt for the oxidation of methanol to formaldehyde and CO_2 can be dramatically and reversibly affected when oxygen anions O^{2-} are electrochemically pumped to or from the Pt catalyst surface. The experiments were conducted using a stabilized zirconia solid electrolyte at temperatures 600 to 900 K. The steady state increases in the catalytic rates of H_2CO and CO_2 formation, are typically 10^3–10^4 higher than the rate of O^{2-} transport to or from the catalyst surface. Over a wide range of experimental conditions the catalytic rates depend exponentially on the catalyst–solid electrolyte overpotential, which is proportional to the induced change in catalyst work function. The product selectivity to H_2CO can be varied between 35 and 60% by controlling the catalyst potential. The phenomena are reversible and show that catalyst work function and catalytic activity and selectivity can be varied at will by adjusting the catalyst potential. As in previous studies of non-Faradaic electrochemical modification of catalytic activity one can interpret the observed behaviour by taking the change in catalyst work function with changing catalyst potential and the concomitant changes in the strength of chemisorptive bonds into account.

INTRODUCTION

Catalytic phenomena on metals can be both studied and influenced by the use of solid electrolyte cells. Work in this area prior to 1988 has been reviewed recently (*1–4*). Earlier studies focused mainly on passive potentiometric measurements of the activity of chemisorbed oxygen on porous metal catalyst films. This technique of Solid Electrolyte Potentiometry (SEP) combined with simultaneous kinetic measurements has been used to study several catalytic reactions on metals (*5–9*). The SEP technique is particularly suitable for studying the mechanism of oscillatory reactions (*1, 10–13*).

However, the "active" use of solid electrolytes to influence catalytic phenomena on metals appears to offer some far more interesting opportunities. In this active mode of operation a current I is applied to cells of the type

$$\text{gaseous reactants, metal catalyst}\,|ZrO_2\,(8\ \text{mol\%}\ Y_2O_3)|M,O_2, \quad (1)$$

and oxygen anions O^{2-} are pumped to or from the catalyst surface at a rate $I/2F$, where F is Faraday's constant. The metal M catalyzes the electrocatalytic reaction

$$O_2(g) + 4e^- \rightleftharpoons 2O^{2-} \quad (2)$$

and serves as a means of supplying or removing O^{2-} to or from the metal catalyst film through the gas-impervious stabilized zirconia solid electrolyte.

It has been known for some years that solid electrolyte cells operating in this active, or oxygen "pump," mode can electrocatalytically promote the rate of several re-

*To whom correspondence should be addressed.

0021-9517/91 $3.00

actions such as NO decomposition (*14, 15*), CO hydrogenation (*16, 17*), methane conversion to C_2 hydrocarbons (*18, 19*), and propylene conversion to acrolein (*20*). In two such studies involving ethylene and propylene epoxidation on Ag (*21–23*) it was observed that the increase in the rates of olefin epoxidation and conversion to CO_2 was typically a factor of 300 higher than the rate $I/2F$ of O^{2-} transport to the Ag catalyst surface. This was the first report of a "non-Faradaic" catalytic rate enhancement.

Very recently this new phenomenon of Non-Faradaic Electrochemical Modification of Catalytic Activity (NEMCA) has been observed and studied systematically for the reactions of CO oxidation on Pt (*24, 28*), ethylene oxidation on Pt (*25, 26*) and on Ag (*28, 29*), CO oxidation on Pd (*28*), methanol dehydrogenation and decomposition on Ag (*25, 27*) and on Pt (*28*), methane oxidation on Pt (*30*), and methane oxidative coupling on Ag (*32*). Dramatic changes in catalytic activity were observed with all these reactions. Table 1 lists the catalytic reactions for which the NEMCA effect has been studied so far and gives typical observed values of the enhancement factor Λ (*1, 24–32*) and rate enhancement ratio ρ (*28–32*). These parameters are defined as

$$\Lambda = \frac{\Delta r}{(I/2F)} \tag{3}$$

$$\rho = r/r_0, \tag{4}$$

where $\Delta r = r - r_0$ is the change in *catalytic* reaction rate, r_0 is the open-circuit, i.e., regular catalytic, rate, and $I/2F$ is the rate of O^{2-} transport to or from the catalyst. As in previous studies (*1, 24–32*), the current I has been defined throughout this paper to be positive when O^{2-} is pumped *to* the catalyst and negative when O^{2-} is pumped *from* the catalyst. As shown in Table 1 enhancement factor Λ values as high as $3 \cdot 10^5$ and rate enhancement ratio ρ values as high as 70 have been measured for some reactions. A catalytic reaction has been defined to exhibit a positive NEMCA effect when $\Lambda \gg 1$ and a negative NEMCA effect when $\Lambda \ll -1$ (*27, 32*).

The central and common findings of all previous studies of the NEMCA effect (*25–32*) can be summarized as follows:

I. Catalytic rates depend exponentially on catalyst potential over wide ranges of experimental conditions.

II. The order of magnitude of the enhancement factor Λ for a given reaction, catalyst, and catalyst–electrolyte interface can be estimated from $2Fr_0/I_0$, where I_0 is the exchange current of the catalyst–electrolyte interface.

III. The catalytic rate relaxation time constants during galvanostatic transients are of the order of $2FN/I$, where N, expressed in gatoms, denotes the total catalytic surface area.

The above observations have been interpreted semiquantitatively by considering the changes induced in the work function of the catalytic surface caused by the development of activation overpotential at the catalyst–solid electrolyte interface (*25–27*). This is also supported by a very recent investigation, involving the oxidation of ethylene on Pt, which showed that the NEMCA effect can also be induced by using β''-Al_2O_3, which is a Na^+ conductor, as the solid electrolyte instead of stabilized zirconia (*31, 32*). Direct experimental proof obtained by measuring the catalyst work function with a Kelvin probe has been obtained very recently (*32*).

In the present work the NEMCA effect is examined for the case of methanol oxidation on Pt. This is a complex catalytic reaction system leading to the formation of H_2CO and CO_2 over the temperature range investigated. The kinetics of this system have been examined in the past on Pt wires (*33–35*). Madix and Abbas (*36*) and Sexton (*37*) have used a variety of surface spectroscopic techniques to investigate the mechanism of CH_3OH decomposition on clean well-characterized Pt(111) surfaces under ultrahigh-vacuum conditions (*36, 37*). Despite the complexity of the kinetics of this system it

TABLE 1

Catalytic Reactions Found to Exhibit the NEMCA Effect

Reactants	Products	Catalyst	Electrolyte	Temperature (°C)	$\Delta r/(I/2F)$	r/r_0	References
I. Positive (electrophobic) NEMCA effect ($\Delta r > 0$ with $I > 0$*, $e\Delta\Phi > 0$)							
C_2H_4, O_2	CO_2	Pt	ZrO_2–Y_2O_3	260–450	$[0, 3 \cdot 10^5]$	<55	(25, 26, 32)
C_2H_4, O_2	CO_2	Pt	β''-Al_2O_3	180–300	$[0, 5 \cdot 10^4]$	<4	(31, 32)
CH_3OH, O_2	H_2CO,CO_2	Pt	ZrO_2–Y_2O_3	300–500	$[0, 10^4]$	<3	This work
CO, O_2	CO_2	Pt	ZrO_2–Y_2O_3	300–550	[0, 500]	<3	(24, 28)
CO, O_2	CO_2	Pd	ZrO_2–Y_2O_3	400–550	$[0, 10^3]$	<1.5	(28)
CH_4, O_2	CO_2	Pt	ZrO_2–Y_2O_3	650–750	[0, 5]	<70	(30)
CH_4, O_2	CO, CO_2, C_2H_4	Ag	ZrO_2–Y_2O_3	650–750	[0, 5]	<30	(32)
C_2H_4, O_2	C_2H_4O, CO_2	Ag	ZrO_2–Y_2O_3	320–470	[0, 300]	<3	(21, 22, 28, 29)
C_3H_6, O_2	C_3H_6O, CO_2	Ag	ZrO_2–Y_2O_3	320–420	[0, 300]	<2	(23, 28)
II. Negative (electrophilic) NEMCA effect ($\Delta r > 0$ with $I < 0$, $e\Delta\Phi < 0$)							
CO, O_2	CO_2	Pt	ZrO_2–Y_2O_3	300–550	$[0, -500]$	<6	(24, 28)
CH_3OH, O_2	H_2CO, CO_2	Pt	ZrO_2–Y_2O_3	300–550	$[0, -10^4]$	<15	This work
CH_3OH	H_2CO, CO, CH_4	Pt	ZrO_2–Y_2O_3	400–500	[0, −10]	<3	(28)
CH_3OH	H_2CO, CO, CH_4	Ag	ZrO_2–Y_2O_3	550–750	[0, −25]	<6	(25, 27)

* Current is defined positive when O^{2-} are supplied to or Na^+ removed from the catalyst surface.
** Change in product selectivity observed.

is found that, as in previous studies (*24–32*), catalytic rates depend exponentially on catalyst potential and work function over wide ranges of experimental conditions. Product selectivity is also found to vary significantly with catalyst potential. An interesting peculiarity of the present system is that it exhibits both positive (electrophobic) and negative (electrophilic) NEMCA behavior; i.e., catalytic rates are enhanced, to a different extent, both by increasing and by decreasing catalyst potential and work function.

EXPERIMENTAL

The experimental apparatus is identical to the one described recently in detail for the study of the NEMCA effect during CH_3OH dehydrogenation and decomposition on Ag (*27*). The only difference is the addition of a third line in the reactor feed system for admixing synthetic air (L' Air Liquid standard synthetic air 20% O_2–80% N_2) with the two other feed streams, one of which is ultrapure (99.999%) He and the other, He saturated with CH_3OH obtained by sparging ultrapure He through a thermostated saturator containing liquid CH_3OH (*27*). By controlling the flow rates of the three feed streams one can vary the methanol partial pressure P_M in the CSTR reactor at constant P_{O_2} and vice versa. The feed and product analysis unit of the CSTR catalytic reactor, involving on-line gas chromatography, mass spectrometry, and IR spectroscopy has also been recently described in detail (*26, 27*).

The atmospheric pressure yttria-stabilized zirconia continuous flow CSTR reactor shown schematically in Fig. 1 has a volume of 30 cm^3 and has been described in detail in previous works (*10, 24, 26–28*).

The porous Pt catalyst film was deposited on the inside bottom wall of the stabilized zirconia tube as described previously (*24,*

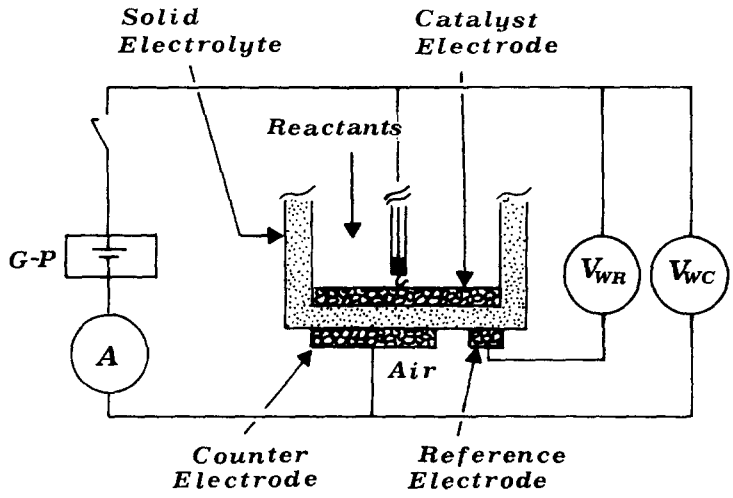

FIG. 1. Electrode configuration and electrical circuit; G–P, galvanostat–potentiostat.

26), i.e., by using a thin coating of Engelhard A1121 Pt paste followed by drying and calcining in air first for 2 h at 400°C and then for 20 min at 820°C. Porous Pt catalyst films deposited in this mode have thicknesses on the order of 5μm and true surface areas on the order of 500 cm^2 and have been shown by *ex situ* XPS to contain no detectable metal impurities (*13, 24*). Typical scanning electron micrographs of such porous Pt catalyst films and of sections perpendicular to the Pt catalyst film-stabilized zirconia interface have been presented in a previous paper (*26*). In the course of the present investigation we used two different catalyst films, denoted by C1 and C2. They both showed qualitatively the same catalytic behaviour. The true surface area of C1 was higher than that of C2 approximately by a factor of 3.

Two similar porous Pt films were deposited on the outside bottom wall of the stabilized zirconia tube, which was exposed to ambient air as shown in Fig. 1. One of the films, with a superficial surface area of 1.2 cm^2, served as the counter electrode, and the other, with a superficial surface area of 0.1 cm^2, served as a reference electrode. An AMEL 553 galvanostat was used to apply constant currents between the catalyst and the counter electrode.

Under open-circuit conditions the film exposed to the reactants acts as a regular catalyst for CH_3OH oxidation to H_2CO and CO_2. The open-circuit emf V_{WR}^0 is typically between -100 and -500 mV over the range of temperature and gaseous compositions used in this study. When the circuit is closed and the galvanostat is used to apply a constant current I between the working and counter electrodes, oxygen anions O^{2-} are transferred to or from the working electrode (catalyst) at a rate $I/2F$. At the same time the catalyst potential relative to the reference electrode V'_{WR} deviates from its open-circuit emf value V_{WR}^0. The difference $V'_{WR} - V_{WR}^0$ ideally equals the overpotential η at the catalyst–solid electrolyte interface (*24, 26, 27*). In practice there is always a small but finite "uncompensated" resistance between the catalyst and the reference electrode and thus V'_{WR} always contains a nonzero ohmic component (*38, 39*). This component, which was typically of the order of 5–30 mV in our system, was determined using the current interruption technique in conjunction with a Hameg HM 205 memory oscilloscope and was subtracted from V'_{WR} in order to obtain the IR-free catalyst potential V_{WR}. This permits accurate measurement of η from

$$\eta = V_{WR} - V_{WR}^0. \qquad (5)$$

The theoretical basis for using η vs I data

to extract the exchange current I_0 of the catalyst–solid electrolyte interface and the anodic and cathodic transfer coefficients α_a and α_c by means of the classical Butler–Volmer equation (*38*) has been discussed in detail previously (*24, 26, 27, 40*).

RESULTS

Regular (Open-Circuit) Catalytic Behaviour

The open-circuit catalytic behaviour of Pt for the oxidation of methanol was studied at temperatures 600 to 900 K. The partial pressures of methanol P_M and of oxygen P_{O_2} were varied in the ranges 10^{-3}–10^{-2} and 0.02–0.2 bar, respectively. The only detectable products were H_2CO and CO_2, with only trace amounts of CO, in agreement with the work of McCabe and McCready (*35*), who found significant CO formation only with methanol-rich mixtures. The total conversion of methanol was kept below 20% in most experiments. A limited study of the effect of residence time on reactor performance was carried out by varying the total flow rate. It was found that the rates r_{0,H_2CO} and r_{0,CO_2} of formaldehyde and CO_2 formation, respectively, were practically unaffected by flow rate. This implies both the absence of any external mass transfer limitations and also that the two reactions

$$CH_3OH + 1/2O_2 \xrightarrow{r_{0,H_2CO}} H_2CO + H_2O \quad (6)$$

$$CH_3OH + \tfrac{3}{2}O_2 \xrightarrow{r_{0,CO_2}} CO_2 + 2H_2O \quad (7)$$

can be treated macroscopically and kinetically as two independent parallel reactions. At higher methanol conversions, the oxidation of H_2CO can, of course, become important (*35*).

Figure 2 shows that over the investigated temperature range both r_{0,H_2CO} and r_{0,CO_2} are rather weakly temperature dependent and that there exist two distinct kinetic regimes below and above 750 K. In the low temperature range both r_{0,H_2CO} and r_{0,CO_2} decrease with increasing T with absolutely small but negative apparent activation energies, i.e.,

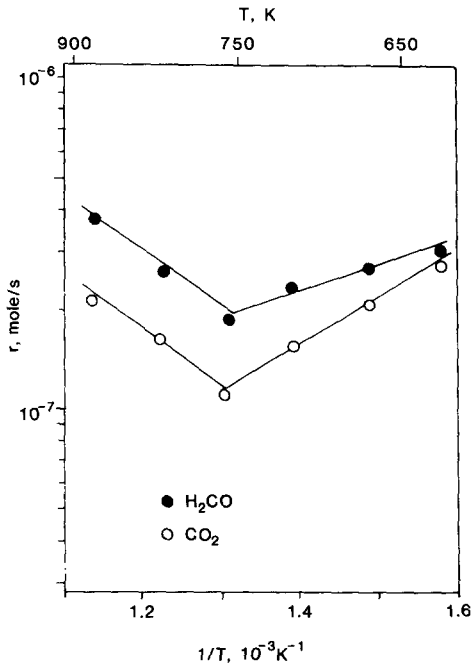

FIG. 2. Effect of temperature on the rates of H_2CO and CO_2 formation; $P_M = 8 \cdot 10^{-3}$ bar, $P_{O_2} = 0.18$ bar; catalyst C1.

−3 and −6 kcal/mole respectively. This "pathological" behaviour is rather rare in heterogeneous catalysis but can, in general, be easily explained within the framework of classical Langmuir–Hinshelwood kinetic models. Previous kinetic studies of this system (*33–35*) were mostly carried out at much lower temperatures than those in the present study and only McCabe and McCready have reported kinetic data in this pathological T range, i.e., 625 to 750 K (*35*). Their data (e.g., Figs. 1, 2, and 4 in Ref. (*35*)) clearly show a negative apparent activation energy for CO_2 formation in this temperature range. Also r_{0,H_2CO} was found by these authors to exhibit negative activation energy between 450 and 500 K (*35*) and to vanish at higher temperatures due to H_2CO oxidation. However, the discussion of activation energies in that work was limited to lower temperatures, where both activation energies are positive (*35*). Above 750 K the behaviour is "normal" (Fig. 2) and both r_{0,H_2CO} and r_{0,CO_2} have activation energies of about 9 kcal/

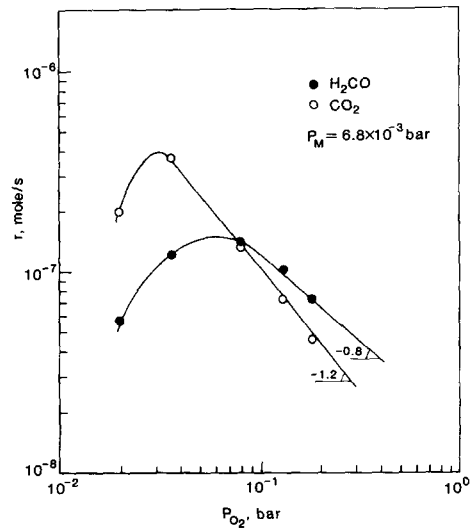

FIG. 3. Effect of p_{O_2} on the rates of H_2CO and CO_2 formation; T = 650 K, $P_M = 6.8 \cdot 10^{-3}$ bar; catalyst C2.

mole. This is, interestingly, very close to the values reported by previous workers (*33–35*) for low temperatures ($T < 625$ K). One may thus conclude from the present and previous kinetic studies (*33–35*) that the apparent activation energies for both H_2CO and CO_2 formation are of the order of 9–10 kcal/mole for both the low ($T < 625$ K) and high ($T > 750$ K) temperature ranges and are weakly negative (3–6 kcal/mole) for the intermediate ($625 < T < 750$ K) temperature range, where most of the present kinetic measurements were taken.

Figures 3 and 4 show the dependence of the open-circuit rates r_{0,H_2CO} and r_{0,CO_2} on P_{O_2} and P_M. Both rates go through a maximum with increasing P_{O_2}. The maximum is more pronounced for r_{0,CO_2}. These rate maxima are indicative of surface reaction rate controlling mechanisms for both reactions, with chemisorbed oxygen competing for surface sites with chemisorbed species resulting from methanol chemisorption. The inhibiting role of oxygen for this system has been already reported by Firth (*33*), who found a $-\frac{1}{2}$ rate dependence on P_{O_2}, but, interestingly, not by Gentry *et al.* (*34*). The study of McCabe and McCready (*35*) was limited to $P_{O_2} < 0.015$ bar, where the rates are of a positive order in oxygen (Fig. 3).

In the region of oxygen inhibition where the effect of P_M was studied (Fig. 4) both rates are proportional to P_M^2 and nearly inversely proportional to P_{O_2}; i.e., they can be approximated by the empirical expressions

$$r_{0,H_2CO} = K_{0,H_2CO} P_M^2 / P_{O_2}^{0.8} \quad (8)$$

$$r_{0,CO_2} = K_{0,CO_2} P_M^2 / P_{O_2}^{1.2}. \quad (9)$$

Previous workers have reported methanol reaction orders varying between -0.17 and $+1$ (*33–35*). The significantly different operating temperatures are the most probable reason for this difference. It is worth pointing out that the kinetics of this system are, apparently, very sensitive to operating conditions and to catalyst pretreatment. For example Firth (*33*) reports a product selectivity to formaldehyde S_{H_2CO} of less than 5% near 300 K, whereas Gentry *et al.* (*34*) find $S_{H_2CO} \approx 50\%$ over the same T range. The data of McCabe and McCready show S_{H_2CO} values near 50% below 450 K (Fig. 2 in Ref. (*35*)) with S_{H_2CO} dropping to zero above 500

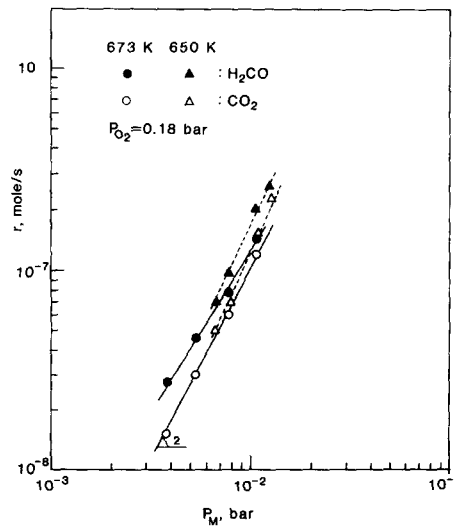

FIG. 4. Effect of methanol partial pressure P_M on the rates of H_2CO and CO_2 formation; p_{O_2} = 0.18 bar; catalyst C2.

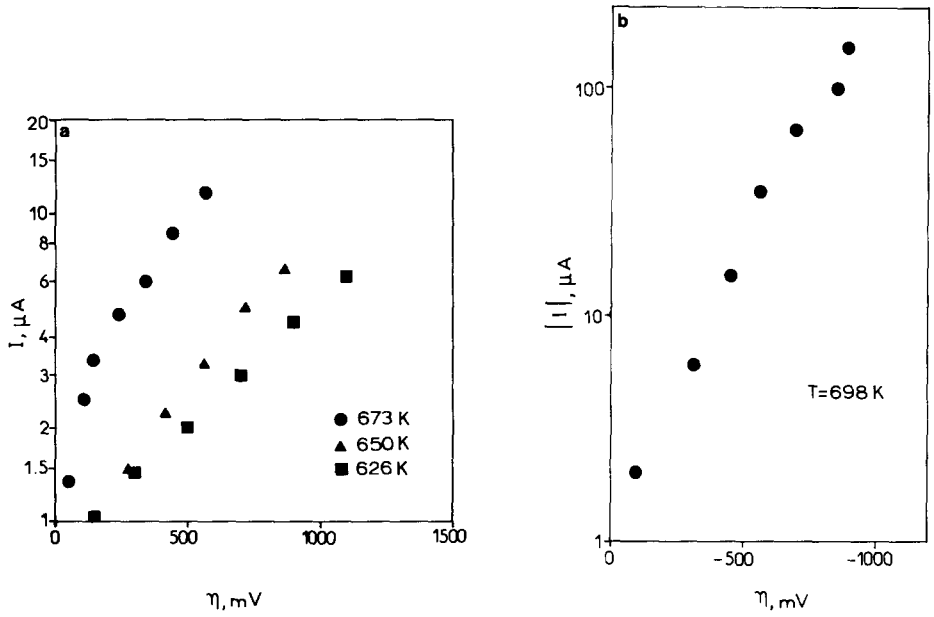

FIG. 5. Typical anodic (a) and cathodic (b) Tafel plots; $P_M = 10^{-2}$ bar, $p_{O_2} = 0.19$ bar; catalyst C2.

K due to H_2CO oxidation (these authors use the term selectivity to denote formaldehyde yield). In the present study, where H_2CO oxidation was suppressed by using short contact times and low methanol conversions, S_{H_2CO} was found to be of the order of 50–60%, as discussed below.

Some mechanistic considerations which can account for the observed open-circuit kinetic behaviour (Figs. 3 and 4) and for the limiting rate expressions (8) and (9) are given under Discussion. The NEMCA effect was studied for $p_{O_2} = 0.17$ to 0.19 bar, i.e., under conditions where the limiting empirical rate expressions (8) and (9) are valid.

Exchange Current Density

Figures 5a and 5b show typical Tafel plots for anodic and cathodic operation, i.e., when O^{2-} are respectively pumped to and from the catalyst surface, which is exposed to methanol and O_2. Both positive ($I > 0$, $\eta > 0$) and negative ($I < 0$, $\eta < 0$) currents lead to Tafel behaviour; i.e., to a quasilinear increase in $\ln|I|$ with increasing $|\eta|$ for $|\eta| > 100$ mV (*26*), according to the Tafel equations

$$\ln(I/I_0) = \alpha_a(F\eta/RT) \qquad (10a)$$

for anodic ($I > 0$, $\eta > 0$) currents and

$$\ln(-I/I_0) = \alpha_c(-F\eta/RT) \qquad (10b)$$

for cathodic ones. The exchange current density $i_0 = I_0/A$, where A is the active solid electrolyte surface area (1.5–2 cm^2 in our experiments) is typically of the order of 1 $\mu A/cm^2$. It was found to increase with temperature with an apparent activation energy of the order of 40 kcal/mole, similarly to previous studies involving Pt catalyst–electrodes (*26, 38*). The anodic and cathodic transfer coefficients are $\alpha_a = 0.14 \pm 0.02$ and $\alpha_c = 0.63 \pm 0.05$, respectively. The value of α_a is significantly lower than that observed during ethylene oxidation on Pt (*26*), i.e., $\alpha_a = 1$. This implies that absorbed species resulting from CH_3OH adsorption must also be involved in the anodic reaction with O^{2-}.

The parameters i_0, I_0, α_a, and α_c refer to the *electrocatalytic* reactions

$$O^{2-} \leftrightharpoons O(a) + 2e^- \qquad (11)$$

$$O^{2-} + CH_3OH \rightarrow \text{products} + 2e^- \qquad (12)$$

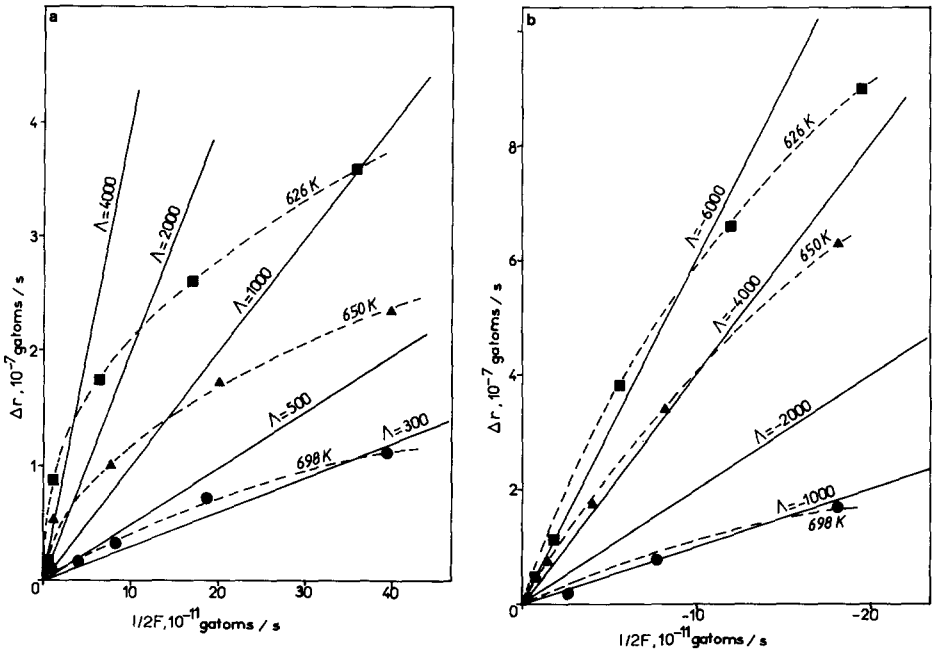

FIG. 6. Effect of positive (a) and negative (b) currents on the increase Δr in the rate of atomic oxygen consumption; catalyst C2. $\Delta r = \Delta r_{H_2CO} + 3\Delta r_{CO_2}$; $P_M = 9 \cdot 10^{-3}$ bar, $P_{O_2} = 0.19$ bar.

which take place at the catalyst–solid electrolyte–gas three-phase boundaries (*26, 27, 38, 40*), and the rates of which, as already mentioned, are several orders of magnitude smaller than the induced changes in the rates of the catalytic reactions (6) and (7). However, these parameters play an important role in understanding the electrocatalytically induced change in catalytic activity, since they determine, together with the current I, the magnitude of the overpotential η, which is proportional to the induced change in catalyst work function (*26, 32*).

NEMCA: Effect of Current

Figure 6a shows the steady-state effect of positive applied current I or, equivalently, the rate of O^{2-} transfer to the catalyst $I/2F$, on the observed increase in the total rate of oxygen consumption due to the increase in the rates of the catalytic reactions (6) and (7). The effect of negative currents, i.e., O^{2-} removal from the catalyst, is shown on Fig. 6b. The solid lines on Figs. 6a and 6b are constant enhancement factor Λ lines. Interestingly, both reactions (6) and (7) exhibit positive NEMCA behaviour (*27*) for positive currents ($I > 0$, $\Delta r > 0$, $\Lambda > 0$) and negative NEMCA behaviour for negative ones ($I < 0$, $\Delta r > 0$, $\Lambda < 0$). The observed enhancement factors Λ are typically of the order of 10^3 for anodic ($I > 0$) operation and of the order of -4×10^3 for cathodic ($I < 0$) operation.

NEMCA: Effect of Overpotential

Figures 7a and 7b show the effect of the catalyst overpotential η on the kinetic constant K_{CO_2} of reaction (7). The effect of η on K_{H_2CO} is qualitatively similar and is not shown in these figures. Below a certain threshold η value, which we denote by η^*_{1,CO_2}, and which is temperature dependent, the rate was found to be practically unaffected, but when η ex-

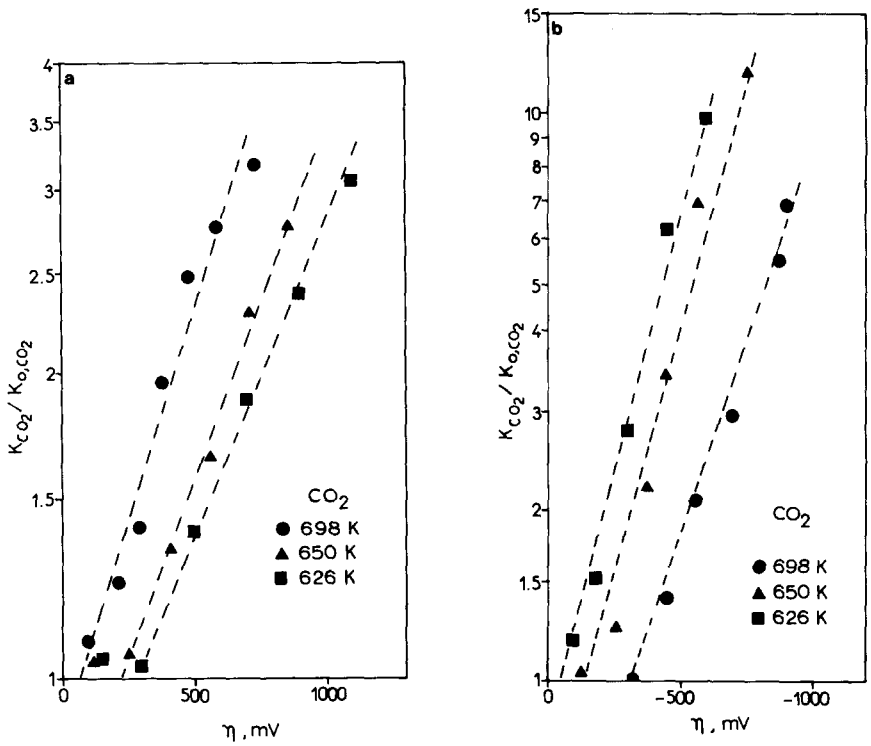

FIG. 7. Effect of overpotential on the rate constant of CO_2 formation for positive (a) and negative (b) currents; conditions as in Fig. 6.

ceeds η^*_{1,CO_2} the rate constant increases exponentially with η; i.e.,

$$\ln(K_{CO_2}/K_{0,CO_2}) = C_1(\eta - \eta^*_{1,CO_2}); \qquad \eta > \eta^*_{1,CO_2}. \quad (13)$$

The constant C_1 is of the order of F/RT, similarly to previous studies of the NEMCA effect, as further discussed below.

For negative currents ($I < 0$, $\eta < 0$) the behaviour is qualitatively similar (Fig. 7b); i.e., decreasing η causes an exponential increase in the rate constant K_{CO_2} below a threshold value η^*_{2,CO_2}:

$$\ln(K_{CO_2}/K_{0,CO_2}) = C_2(\eta^*_{2,CO_2} - \eta). \quad (14)$$

The behavior for K_{H_2CO}, which increases exponentially with η above and below, respectively, two threshold values η^*_{1,H_2CO} and η^*_{2,H_2CO}, is similar. As shown in Figs. 7a and 7b, the parameters η^*_{1,CO_2} and η^*_{2,CO_2} are strongly temperature dependent. The same applies to the corresponding parameters for K_{H_2CO}. However, as shown below, all the results can be unified when they are examined as a function of catalyst potential V_{WR} instead of overpotential η.

Effect of Catalyst Potential V_{WR}

The observed threshold η^*_1, η^*_2 values are temperature dependent, but so is the open-circuit emf $V^0_{WR} = V_{WR}(I = 0)$. It was found that the differences between η^*_1, η^*_2 and V^0_{WR} cancel out, so that when the kinetic constants are examined at the same potential $V_{WR} = V^0_{WR} + \eta$, or, more generally, at the same dimensionless potential $\Pi = FV_{WR}/RT$, then all the results obtained at different temperatures practically coincide. This can

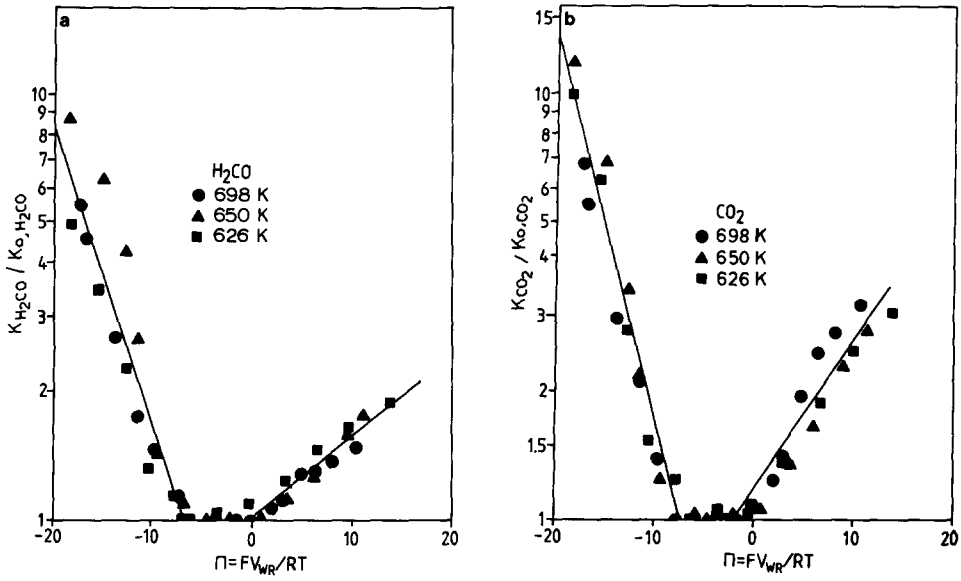

FIG. 8. Effect of dimensionless catalyst potential Π on the rate constants of H_2CO (a) and CO_2 (b) formation; conditions as in Fig. 6.

be seen in Figs. 8a and 8b, which show conclusively, in conjunction with Figs. 7a and 7b, that catalyst potential V_{WR} and $\Pi = FV_{WR}/RT$ are the most relevent parameters for describing the NEMCA effect, rather than the overpotential η.

The same figures show that decreasing the catalyst potential leads to rate enhancement ratios ρ as high as 8 and 15 for H_2CO and CO_2 formation, respectively, i.e., to rate enhancements of 800 and 1500%, respectively, for the two reactions, while increasing V_{WR} causes more moderate rate enhancement, i.e., ρ values of the order of 2 and 3, respectively, for H_2CO and CO_2 formation.

All the data can be approximated by

$$\ln(K_{H_2CO}/K_{0,H_2CO}) = \alpha_{1,H_2CO}(\Pi - \Pi^*_{1,H_2CO}), \quad \Pi^*_{1,H_2CO} < \Pi, \quad (15a)$$

$$K_{H_2CO} = K_{0,H_2CO}, \quad \Pi^*_{2,H_2CO} < \Pi < \Pi^*_{1,H_2CO}, \quad (15b)$$

$$\ln(K_{H_2CO}/K_{0,H_2CO}) = \alpha_{2,H_2CO}(\Pi - \Pi^*_{2,H_2CO}), \quad \Pi < \Pi^*_{2,H_2CO}, \quad (15c)$$

for H_2CO formation and by

$$\ln(K_{CO_2}/K_{0,CO_2}) = \alpha_{1,CO_2}(\Pi - \Pi^*_{1,CO_2}), \quad \Pi^*_{1,CO_2} < \Pi, \quad (15d)$$

$$K_{CO_2} = K_{0,CO_2}, \quad \Pi^*_{2,CO_2} < \Pi < \Pi^*_{1,CO_2}, \quad (15e)$$

$$\ln(K_{CO_2}/K_{0,CO_2}) = \alpha_{2,CO_2}(\Pi - \Pi^*_{2,CO_2}), \quad \Pi < \Pi^*_{2,CO_2}, \quad (15f)$$

for the formation of CO_2. The dimensionless parameters Π^*_{1,H_2CO}, Π^*_{2,H_2CO}, Π^*_{1,CO_2}, and Π^*_{2,CO_2} are defined as

$$\Pi^*_{1,H_2CO} = F(V^0_{WR} + \eta^*_{1,H_2CO})/RT \quad (16a)$$

$$\Pi^*_{2,H_2CO} = F(V^0_{WR} + \eta^*_{2,H_2CO})/RT \quad (16b)$$

$$\Pi^*_{1,CO_2} = F(V^0_{WR} + \eta^*_{1,CO_2})/RT \quad (16c)$$

$$\Pi^*_{2,CO_2} = F(V^0_{WR} + \eta^*_{2,CO_2})/RT \quad (16d)$$

and take the values $\Pi^*_{1,H_2CO} = -0.5$, Π^*_{2,H_2CO}

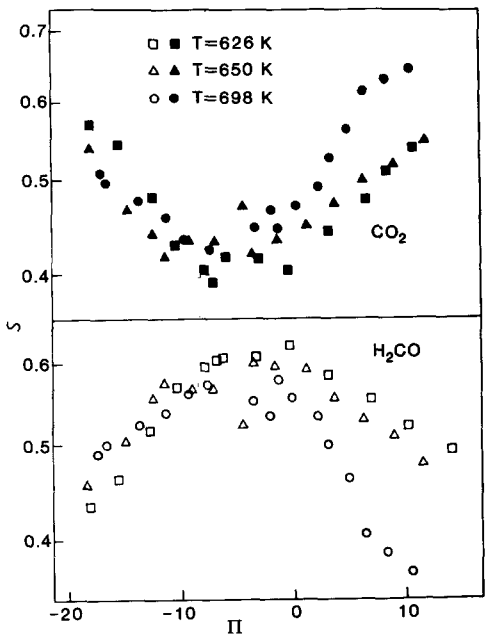

FIG. 9. Effect of dimensionless catalyst potential Π on the product selectivity to CO_2 and H_2CO; conditions as in Fig. 6.

$= -6.8$, $\Pi^*_{1,CO_2} = -0.2$, and $\Pi^*_{2,CO_2} = -7.4$. The values of the slope parameters α are $\alpha_{1,H_2CO} = 0.043$, $\alpha_{2,H_2CO} = -0.16$, $\alpha_{1,CO_2} = 0.087$, and $\alpha_{2,CO_2} = -0.21$. It is interesting to note that, despite the complexity of the open-circuit kinetics of this reaction system, its NEMCA behaviour can still be described by the same type of simple expressions (Eqs. (15)) found to describe the NEMCA behaviour of previously studied systems (*25–31*).

Figure 9 shows the effect of the dimensionless catalyst potential Π on the selectivity to H_2CO and CO_2. The open-circuit conditions correspond to $\Pi \approx -4$. It can be seen that both increasing V_{WR}, i.e., positive currents, and decreasing V_{WR}, i.e., negative currents, cause a decrease in the selectivity to formaldehyde; i.e., maximum selectivity to formaldehyde is obtained near the open-circuit conditions. Formally, this is due to the absolutely larger NEMCA coefficient values for CO_2 formation ($\alpha_{1,CO_2} = 0.087$, $|\alpha_{2,CO_2}| = 0.21$) than for H_2CO formation ($\alpha_{1,H_2CO} = 0.043$, $|\alpha_{2,H_2CO}| = 0.16$). A possible physical explanation for this behaviour is given under Discussion.

DISCUSSION

Main Results

1. The catalytic rates of CH_3OH partial oxidation to H_2CO and complete oxidation to CO_2 on Pt can be reversibly enhanced by a factor of 2 and 3, respectively, by supplying oxygen anions to the Pt catalyst surface. The two catalytic rates can also be reversibly enhanced by a factor of 10 and 15, respectively, by removing oxygen anions from the Pt catalyst surface.

2. The open-circuit kinetic behaviour is rather complex, yet the NEMCA-induced change in the apparent kinetic constants is quite simple and conforms to the general form of the NEMCA equation; i.e.,

$$\ln(K/K_0) = \alpha F(V_{WR} - V^*_{WR})/RT, \quad (17)$$

where α and V^*_{WR} are reaction- and catalyst-specific parameters.

Since it has been recently found both theoretically (*26, 27*) and experimentally by means of a Kelvin probe (*32*) that for solid electrolyte cells with electrodes made of the same metal,

$$e\Delta V_{WR} = \Delta e\Phi, \quad (18)$$

where $e\Phi$ is the average work function of the gas-exposed catalyst surface, it follows that Eq. (17) can also be written in the form

$$\ln(K/K_0) = \alpha e(\Phi - \Phi^*)/k_bT, \quad (19)$$

where Φ^* is, again, a catalyst- and reaction-specific constant.

3. The observed enhancement factors Λ are typically of the order of 10^3 for positive currents and $-4 \cdot 10^3$ for negative ones; i.e., both reactions exhibit positive, or "electrophobic" (*27*), NEMCA behaviour at high catalyst potentials and negative, or "electrophilic" (*27*), NEMCA behaviour at low negative potentials. As in previous studies of the NEMCA effect (*25–31*) the order of

magnitude of $|\Lambda|$ can be estimated from $|\Lambda| = 2Fr_0/I_0$, where I_0 is the catalyst–electrolyte exchange current.

4. The selectivity to H_2CO can be varied deliberately between 35 and 60% by adjusting the catalyst potential and goes through a maximum near the open-circuit potential value.

Mechanistic Considerations

Before attempting to interpret the effect of changing catalyst potential and work function on the kinetics of the reactions of H_2CO and CO_2 formation, i.e., the NEMCA effect, it is useful to discuss the open-circuit kinetic behaviour (Figs. 3 and 4). Extraction of mechanistic information from kinetic data can only be speculative, particularly when, as in the present case, the kinetic investigation is not exhaustive enough. However, one can take advantage of (a) previous TPD and surface spectroscopic studies on Pt(111) under UHV conditions (*36, 37*) and (b) methanol oxidation experiments utilizing $^{18}O_2$ (*35*), in order to examine how the observed kinetic behaviour can be fitted within the framework of Langmuir–Hinshelwood–Hougen–Watson (LHHW) models, first under open-circuit and then under NEMCA conditions.

The first problem is the interpretation of the apparent second-order dependence of both rates on P_M. As previously discussed this is the only kinetic feature of the present work which is distinctly different from the results of previous atmospheric pressure studies at lower temperatures (*33–35*). The difference may be due to the substantially different operating temperatures. Also perhaps intrusion of some diffusional falsification, which would make both rates near first order, cannot be safely excluded in some of the early studies utilizing Pt wires, particularly in view of some of the reported abrupt ignition–extinction phenomena (*35*). There are two ways to interpret the observed second-order rate dependence. One is to invoke a strong attractive lateral interaction between adsorbed methoxy groups and also between adsorbed formaldehyde molecules (*36*). A problem with such an interpretation is that adsorbed methoxy groups are rather unstable on Pt (*37*), unlike on Ag or Cu (*36, 37*). Also this type of lateral interaction cannot be modeled conveniently within the framework of LHHW kinetics. We have thus chosen to adopt the second interpretation, which is based on the formation of an adsorbed C_2 species. Indeed Abbas and Madix (*36*) have clearly demonstrated the presence of methyl formate $HCOOCH_3$ both on Pt(111) catalyst surfaces and in the gas phase as a product. These authors observed $HCOOCH_3$ formation only upon dosing the Pt(111) surface with H_2CO, but in the present atmospheric pressure study there is, of course, always enough H_2CO in the gas phase, even at very low methanol conversions, to cause $HCOOCH_3$ formation. It is noteworthy that Abbas and Madix found that $HCOOCH_3$ formation is strongly hindered by coadsorption of S (*36*), which is reminiscent of the observed kinetic hindrance of both rates by chemisorbed oxygen (Fig. 3).

The TPD spectra of Abbas and Madix show that $HCOOCH_3$ is more strongly bonded to the Pt catalyst surface than CH_3OH and H_2CO (*36*). The heat of adsorption of $HCOOCH_3$ was estimated to be 19.3 kcal/mole and its desorption peak temperature was only 50 K below that of chemisorbed CO (*36*). These desorption temperatures (338 and 392 K, respectively, for $HCOOCH_3$ and CO) are, of course, much lower than the temperatures used in the present study, but the enormously higher operating pressure of the present study can compensate for this difference. Finally the fact that the amount of desorbed $HCOOCH_3$ was found in the study of Abbas and Madix to be smaller by a factor of 7 and 23, respectively, than the amounts of desorbed CH_3OH and H_2CO does not in any way contradict the kinetic scheme presented below, since $HCOOCH_3$ desorption could also take place via decomposition to H_2CO and CH_3OH.

It thus appears that $HCOOCH_3$ formation provides the most plausible explanation for the observed second-order rate dependence on P_M. Adsorbed $HCOOCH_3$ could form from the following steps, most of which have been already proposed by Abbas and Madix (*36*):

$$CH_3OH(g) \leftrightharpoons CH_3OH(a) \quad (20a)$$

$$CH_3OH(a) \leftrightharpoons CH_3O(a) + H(a) \quad (20b)$$

$$CH_3O(a) \leftrightharpoons H_2CO(a) + H(a) \quad (20c)$$

$$2H_2CO(a) \leftrightharpoons HCOOCH_3(a) \quad (20d)$$

If equilibrium is established for steps (20a)–(20d), which is a very reasonable assumption for the high operating temperatures of this study, then one can denote this sequence of steps by the overall equilibrium reaction

$$2CH_3OH(g) \leftrightharpoons HCOOCH_3(a) + 4H(a) \quad (21)$$

Within the context of the proposed kinetic model, but also on the basis of the UHV literature (*36, 37*), it may also be assumed that the coverages of $CH_3OH(a)$, $H_2CO(a)$, and methoxy groups $CH_3O(a)$ are rather low, so that $HCOOCH_3(a)$ and O(a), resulting from $O_2(g)$ chemisorption, are the only kinetically important adsorbed species present in significant coverages. That the coverages of $CH_3OH(a)$ and $H_2CO(a)$ are small in comparison to the coverage of $HCOOCH_3(a)$ at elevated temperatures follows directly from the TPD spectra of Abbas and Madix (*36*). Also the results of Sexton (*37*) provide strong evidence that the coverage of $CH_3O(a)$ must also be extremely small.

There may also be some carbon on the surface, as suggested both by Madix under UHV conditions (*36*) and by McCabe at higher pressures (*35*). This carbonaceous species accounts for less than 1% of the rate of CO_2 formation, as shown using $^{18}O_2$ (*35*). However, the role of this secondary pathway can become important under NEMCA conditions, as discussed below.

One can thus postulate that H_2CO and CO_2 are produced primarily by the steps

$$HCOOCH_3(a) \xrightarrow{O(a)} 2H_2CO(g) \quad (22)$$

$$HCOOCH_3(a) + O(a) + s \longrightarrow P \xrightarrow{3\,O(a)} 2CO_2 + 2H_2O \quad (23)$$

Step (22) is assumed to be catalyzed by chemisorbed oxygen O(a). This is reasonable since each O(a) locally increases the surface work function (WF) and can facilitate desorption of electron-acceptor adsorbates. In step (23) a vacant adjacent site s is assumed to be necessary for the formation of a reactive intermediate P, which is further rapidly oxidized to CO_2 and H_2O. The reason for making this assumption becomes apparent below.

Assuming equilibrium for dissociative oxygen chemisorption one can write the following expressions for the rates of the rate controlling steps (22) and (23) or, equivalently, for the rates of the overall reactions (6) and (7):

$$r_{0,H_2CO} = K^0_{H_2CO}\,\theta_f\theta_O \quad (24)$$

$$r_{0,CO_2} = K^0_{CO_2}\,\theta_f\theta_O\theta_v, \quad (25)$$

where the methyl formate (θ_f), oxygen (θ_O), and vacant site (θ_v) coverages are given from the following expressions in terms of the equilibrium constant K_f of reaction (21) and the dissociative oxygen adsorption equilibrium constant K_0:

$$\theta_f = K_f P_M^2 \theta_v \quad (26a)$$

$$\theta_O = K_0 P_{O_2}^{1/2}\,\theta_v \quad (26b)$$

$$\theta_v = 1/(1 + K_f P_M^2 + K_0 P_{O_2}^{1/2}). \quad (26c)$$

On the basis of this model one can physically interpret the observed apparent negative activation energies as being due to the rapid exponential decrease in θ_f, but also in θ_O, with decreasing $1/T$, which can counterbalance the corresponding exponential Arrhenius dependences of the rate coefficients $K^0_{H_2CO}$, $K^0_{CO_2}$ (Eqs. (24) and (25)) if the sum

of the heats of adsorption of oxygen and $HCOOCH_3$ exceeds the corresponding true activation energies of the rate limiting steps (22) and (23). Furthermore, if it is assumed that the coverage of $HCOOCH_3$ is small, which is a reasonable assumption on the basis of Ref. (*36*), then Eqs. (24)–(26) can be written

$$r_{0,H_2CO} = K^0_{H_2CO} K_f K_0 P^2_M P^{1/2}_{O_2} / (1 + K_0 P^{1/2}_{O_2})^2 \quad (27a)$$

$$r_{0,CO_2} = K^0_{CO_2} K_F K_0 P^2_M P^{1/2}_{O_2} / (1 + K_0 P^{1/2}_{O_2})^3. \quad (27b)$$

These equations are in good qualitative agreement with experiment (Figs. 3 and 4). They explain:

I. The second-order rate dependence of both rates on methanol partial pressure.

II. The rate maxima with increasing P_{O_2}. According to Eqs. (27), r_{0,H_2CO} is maximized at $P_{O_2} = 1/K_0^2$, while r_{0,CO_2} is maximized at $P_{O_2} = 1/4K_0^2$. This is in excellent qualitative agreement with experiment (Fig. 3) since r_{0,H_2CO} is maximized at higher P_{O_2} values than r_{0,CO_2}. This was one reason for postulating the need for a vacant site in step (23). Another reason follows immediately:

III. The negative-order dependence of both rates on P_{O_2} for high P_{O_2} values and the observed stronger inhibitive effect of oxygen for the rate of CO_2 formation (Fig. 3). Under these conditions Eqs. (27) reduce to

$$r_{0,H_2CO} = (K^0_{H_2CO} K_f / K_0) P^2_M / P^{1/2}_{O_2} \quad (28a)$$

$$r_{0,CO_2} = (K^0_{CO_2} K_f / K_0^2) P^2_M / P_{O_2}, \quad (28b)$$

which correctly predict a steeper decrease in r_{0,CO_2} than in r_{0,H_2CO} with increasing P_{O_2} (Fig. 3).

It is worth noting that, according to Eqs. (28), in the region of oxygen inhibition the apparent activation energies for H_2CO and CO_2 formation must equal $E^0_{H_2CO} - \Delta H_{O_2}/2 + \Delta H_f$ and $E^0_{CO_2} - \Delta H_{O_2} + \Delta H_f$, respectively, where $E^0_{H_2CO}$, $E^0_{CO_2}$ stand for true activation energies of steps (22) and (23), $-\Delta H_{O_2}$ (>0) is the heat of adsorption of oxygen, and ΔH_f (<0) is the heat of the exothermic overall chemisorptive step (21). Thus, according to the model, both activation energies can become negative, as experimentally observed, if ΔH_f is sufficiently negative.

The above LHHW-type model provides a qualitative explanation for all the features of the observed kinetic behaviour. However, no attempt was made to fit the model into the experimental data. This would not be meaningful in view of the fact that, as discussed below, one of the basic assumptions of Langmuir isotherms, i.e., that of constancy of the heats of adsorption with changing coverages and, therefore, changing catalyst work function, is clearly not fulfilled. The values of the kinetic constants K_{0,H_2CO} and K_{0,CO_2} used in the subsequent discussion are computed from the experimental phenomenological rate expressions (8) and (9).

Origin of NEMCA Effect and of Exponential Dependence of Catalytic Rates on V_{WR}

The proposed explanation of the NEMCA effect is based on the changes induced in the work function of the catalytically active metal surface with changing catalyst potential upon polarization of the metal–electrolyte interface and on the concomitant changes in the heats of chemisorption of adsorbates with changing catalyst work function (*25–32*).

In brief, it has been shown (*26, 27*) that the catalyst potential with respect to the reference electrode, i.e., V_{WR} is given by

$$V_{WR} = (\bar{\mu}_{e,R} - \bar{\mu}_{e,W})/e = (\Phi_W - \Phi_R) + (\Psi_W - \Psi_R), \quad (29)$$

where $\bar{\mu}_{e,W}$, $\bar{\mu}_{e,R}$; $e\Phi_W$, $e\Phi_R$; and Ψ_W, Ψ_R are the electrochemical potentials of electrons (or Fermi levels), work functions, and outer (Volta) potentials, respectively, of the catalyst (W) and reference (R) electrodes. The physical meaning of the various terms appearing in Eq. (29) is depicted schematically

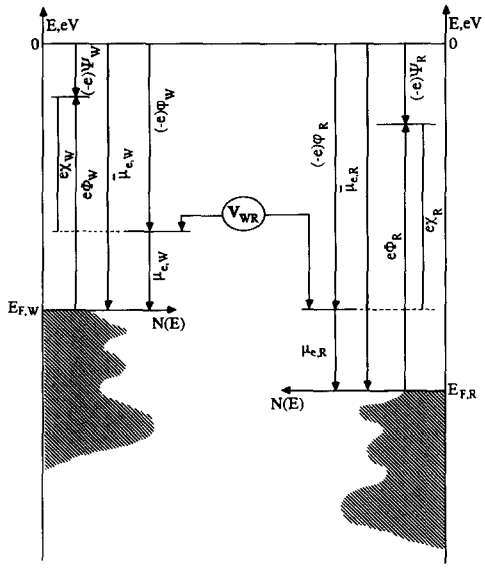

FIG. 10. Schematic representation of the density of states $N(E)$ in the conduction band and of the definitions of work function $e\Phi$, chemical potential of electrons μ_e, electrochemical potential or Fermi level of electrons $\bar{\mu}_e$, surface potential χ, Galvani (or inner) potential φ, and Volta (or outer) potential Ψ for the catalyst (W) and reference electrode (R). The measured potential difference V_{WR} is by definition the difference in Galvani potentials; φ, μ_e, and $\bar{\mu}_e$ are spatially uniform; $e\Phi$ and Ψ can vary locally on the metal sample surfaces; and the Ψ potentials vanish, on the average, for the gas-exposed catalyst and reference electrode surfaces.

in Fig. 10. The Ψ, or Volta, potentials are nonzero only when there is a net charge on the metal catalyst plus adsorbed layer. Consequently the Ψ terms are frequently neglected in the catalytic literature. Equation (29) is valid under both open-circuit and closed-circuit conditions. For open-circuit, i.e., SEP, measurements, it implies that the open-circuit emf V^0_{WR} provides a measure of the catalyst work function in relation to the reference electrode work function, provided no *net* charge develops on the gas-exposed catalytically active surfaces of the two electrodes, i.e., $\Psi_W = \Psi_R = 0$.

Under closed-circuit conditions, i.e., during O^{2-} pumping, the reference electrode remains unaffected; i.e., $\bar{\mu}_{e,R}$, Φ_R and Ψ_R remain constant. One can therefore rewrite Eq. (29) in the form

$$\eta = V_{WR} - V^0_{WR} = (\bar{\mu}_{e,W(I=0)} - \bar{\mu}_{e,W(I)})/e = (\Phi_{W(I)} - \Phi_{W(I=0)}) + (\Psi_{W(I)} - \Psi_{W(I=0)}). \quad (30)$$

The electrochemical potential (or Fermi level) $\bar{\mu}_e$ is spatially uniform throughout the conductive catalyst. The work function $e\Phi_W$ and Volta potential Ψ_W need not be spatially uniform over the catalyst–electrode surface. However, the sum $\Phi_W + \Psi_W$, which equals $-\bar{\mu}_{e,W}/e$, has to be spatially uniform.

As shown schematically in Fig. 11 the surface of a catalyst electrode deposited on a solid electrolyte is divided in two distinct parts. One part, which usually accounts for less than 1% of the total catalyst electrode surface area, is in contact with the electrolyte. The second part is in contact with the gas phase and constitutes the catalytically active surface. In the subsequent discussion as well as on Fig. 11 we use the subscripts 1 and 2 to denote quantities referring to the

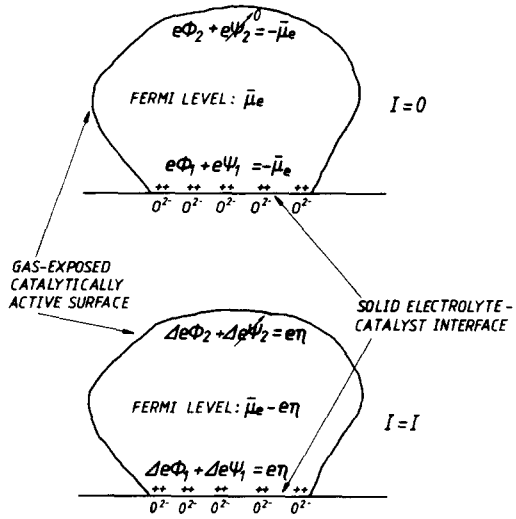

FIG. 11. Schematic representation of a metal crystallite deposited on stabilized zirconia and of the changes induced in its electronic properties upon polarizing the catalyst–electrolyte interface and changing the Fermi level (or electrochemical potential) from an initial value $\bar{\mu}_e$ to a new value $\bar{\mu}_e - e\eta$.

catalyst–electrolyte and catalyst–gas interfaces, respectively, and we consider as the control volume the catalyst electrode plus the adsorbed species on the catalyst–gas interface.

It follows from simple electrostatic considerations that, since there can be no net charge in the gas phase, any net charge on the catalyst electrode will be localized at the catalyst–solid electrolyte interface, facing an equal and opposite charge in the solid electrolyte. Any ions or molecules directly adsorbing on the catalytically active surface will be paired with a compensating charge in the metal. Consequently $\Psi_2 = 0$ under both open-circuit and closed-circuit conditions.

It is worth pointing out that in the present discussion Φ_2 and Ψ_2 stand for the *average* work function and Volta potential of the gas-exposed catalytic surface. Some nontrivial spatial variation in the local work function and, consequently, the Volta potential can be expected for any real polycrystalline film surface, since different crystallographic planes will, in general, have different work function values. This, in conjunction with the constancy of the Fermi level, dictates that, in general, slightly different nonzero excess free charge densities will exist on different planes, causing local variations in Ψ_2. Surface physicists would refer to this as a local variation in the "vacuum level." However, since $\Phi_2 = \Sigma f_i \Phi_i$, where f_i is the total catalyst surface fraction corresponding to a crystallographic plane with a work function Φ_i (*41, 42*) it will also be that $\Psi_2 = \Sigma f_i \Psi_i = 0$. These local spatial variations in Φ_2 and Ψ_2 are not expected to be significant in polycrystalline films with large (~ 1 μm) crystallites, such as the ones used in this and in other NEMCA studies, since the surface must consist primarily of low Miller index planes and in particular of the (111) plane.

When the catalyst–electrolyte interface gets polarized by O^{2-} pumping to or from the catalyst and the Fermi level of the catalyst changes from an original value $\bar{\mu}_e$ to a new value $\bar{\mu}_e - e\eta$, it follows from Eq. (30) that

$$\eta = \Delta\Phi_1 + \Delta\Psi_1 = \Delta\Phi_2 + \Delta\Psi_2. \quad (31)$$

But as already discussed, $\Psi_2 = 0$, and therefore $\Delta\Psi_2 = 0$. Consequently $\eta = \Delta\Phi_2$; i.e., the electrochemically measurable quantity $e\eta$ equals the change $e\Delta\Phi_2$ in the work function of the catalytically active surface. Therefore, when the Φ and Ψ terms in Eqs. (29) and (30) refer to the catalytically active surface, then these equations reduce to the form

$$V_{WR} = \Phi_W - \Phi_R \quad (32)$$

$$\eta = V_{WR} - V^0_{WR} = \Phi_{W(I)} - \Phi_{W(I=0)}. \quad (33)$$

Experimental verification of Equations (32) and (33) has been obtained recently by directly measuring the work function of a catalyst electrode using a Kelvin probe under reaction conditions (*32*).

Equation (*33*) implies that when $\eta > 0$, i.e., when $V_{WR} > V^0_{WR}$ or, equivalently, when O^{2-} is pumped to the catalyst, then there is an increase in the catalyst work function. This has been found to cause dramatic non-Faradaic increases in the rates of C_2H_4 and C_3H_6 epoxidation and complete oxidation on Ag (*21–23, 29*), CO oxidation on Pt (*24, 28*) and complete C_2H_4 oxidation on Pt (*26, 28*). When $\eta < 0$, i.e., when $V_{WR} < V^0_{WR}$ or, equivalently, when O^{2-} is pumped from the catalyst surface, then Eq. (33) implies a decrease in catalyst work function. This has been found to cause significant non-Faradaic increases in the rates of CH_3OH dehydrogenation and decomposition on Ag (*27*) and on Pt (*28*).

When the catalyst work function changes, the strengths of the chemisorptive bonds are also expected to change significantly. Boudart was the first to tackle this problem with a semiempirical electrostatic model (*43*) according to which

$$\Delta(-\Delta H_a) = -(n/2)e\Delta\Phi, \quad (34)$$

where $-\Delta H_a$ is the heat of chemisorption

of a covalently bonded adsorbate and n is the number of valence electrons of the adsorbate taking part in the chemisorptive bond. Despite the semiempirical nature of Eq. (34), for which it has been criticized (*44*), it has been found in several occasions to be in reasonable agreement with experiment (*43*) and also to provide a simple interpretation for the observed linear variation of activation energy with work function in NEMCA studies over relatively wide (0.3–1 eV) ranges of work function (*26, 28, 32*). Within the context of Boudart's early electrostatic model heats of adsorption are always predicted to decrease regardless of the sign of $\Delta\Phi$; i.e., $|\Delta\Phi|$ should replace $\Delta\Phi$ in Eq. (34). However, for the case of electron acceptor adsorbates an increase (or decrease) in work function causes a decrease (or increase) in the availability of metal electrons for chemisorptive bond formation via increased occupancy of bonding chemisorptive bond orbitals; therefore it would appear preferable to retain Boudart's equation in the form of Eq. (34). It would also appear, through the same qualitative reasoning, that for the case of electron donnor adsorbates the minus sign should be omitted in Eq. (34) or, equivalently, n in Eq. (34) should stand for the number of electrons donated by the metal to the adsorbate so that it would be taken as a negative number when electrons are donated to the metal by the adsorbate. The same qualitative conclusions can be reached from the more modern theoretical considerations of Shustorovich (*45*), who expresses the metal–adsorbate bond strength in terms of the differences $E_F - \varepsilon_A$ and $\varepsilon_A^* - E_F$, where E_F is the metal Fermi level, ε_A is energy of the higher occupied (σ or π) adsorbate orbital, and ε_A^* is the energy of the lowest unoccupied (σ^* or π^*) adsorbate orbital. All these are, of course, oversimplifications since chemisorptive bonds frequently involve both donation and backdonation of electrons in different orbitals (e.g., CO chemisorption on transition metals (*46*)). NEMCA offers the possibility of directly examining the effect of work function on heats of adsorption and work on this subject is in preparation (*47*). We base the following qualitative discussion on Eq. (34), although both experimental heat of adsorption vs work function data at constant adsorbate coverage and more specific theoretical treatments are highly desirable.

Reactions Exhibiting Positive and Negative NEMCA Behaviour

The reactions for which the NEMCA effect has been studied so far (Table 1) can be divided into two groups: those exhibiting "positive" NEMCA behaviour, i.e., $\Lambda > 0$ or, equivalently, rate acceleration with increasing catalyst work function, and those exhibiting "negative" NEMCA behaviour, i.e., $\Lambda < 0$ or, equivalently, rate acceleration with decreasing catalyst work function. The terms electrophobic and electrophilic, respectively, have been proposed for these two groups of reactions (*27*). Similarly to CO oxidation on Pt under reducing conditions (*24*), the oxidation of CH_3OH to H_2CO and CO_2 exhibits both positive and negative NEMCA behaviour; i.e., it behaves as an electrophobic reaction at high catalyst potentials and as an electrophilic reaction at low catalyst potential values.

When the rate limiting step of a catalytic reaction involves cleavage of a metal–electron acceptor adsorbate bond, then one would expect that, provided the nature of the activated complex is not changing, the rate of the reaction will increase exponentially with $-(-\Delta H_{ad})$ and with V_{WR} and $e\Delta\Phi$; i.e., one would expect the reaction to exhibit positive or electrophobic NEMCA behaviour. This indeed appears to be the case for the electrophobic reactions listed in Table 1. Their rate limiting steps indeed involve cleavage of metal–oxygen bonds (*26, 28*).

If, in the other hand, the rate limiting step of a catalytic reaction involves cleavage of an intraadsorbate bond in an electron acceptor adsorbate, e.g., methanol dehydro-

genation and decomposition on Ag (*27*), then one would expect the reaction to exhibit negative or electrophilic NEMCA behaviour, since from classical bond-order conservation considerations the strengthening of a metal–adsorbate bond due to a decrease in work function causes a weakening in the intraadsorbate bond strengths and a concomitant increase in catalytic rate. Indeed, all reaction found so far to exhibit negative NEMCA behaviour are dehydrogenation or decomposition reactions. The oxidation of CO, which exhibits negative NEMCA behaviour at very negative catalyst potentials and reducing environments, is no exception to this rule since under these conditions the reaction proceeds via CO disproportionation on the catalyst surface followed by carbon combustion (*24*).

In view of the previous discussion one can interpret the observed NEMCA behaviour of methanol oxidation to H_2CO and CO_2 as follows:

Increasing V_{WR} or $e\Phi$ causes a decrease in the binding energy of the chemisorptive bonds of atomic oxygen and also probably of methyl formate; consequently both adsorption coefficients K_0 and K_f decrease. According to Eq. (34) and in view of the fact that the number n of metal conduction electrons participating in the chemisorptive bond is two for the case of O(ad) and probably 1 for the case of methyl formate, it follows that the decrease in the heat of adsorption of oxygen will be more pronounced. Consequently K_0 will decrease faster than K_f with increasing potential. This by itself would suffice to explain the observed increase in the phenomenological rate coefficients $K_{H_2CO} = K^0_{H_2CO}(K_f/K_0)$ and $K_{CO_2} = K^0_{CO_2}(K_f/K_0^2)$ with increasing potential. However, since the rate limiting steps of both reactions involve cleavage of metal—oxygen bonds, albeit with simultaneous formation of new chemisorptive bonds, it is quite likely that the rate constants $K^0_{H_2CO}$ and $K^0_{CO_2}$ are also increasing with increasing potential, thus further contributing to the observed increase in the phenomenological rate constants K_{H_2CO} and K_{CO_2}.

Since increasing catalyst work function causes a loosening in the metal–oxygen bond and a concomitant decrease in the oxygen chemisorption equilibrium constant K_0, it follows from Eqs. (28) that the selectivity to H_2CO will decrease with increasing catalyst work function, as is experimentally observed. Physically this is because CO_2 formation, which according to the proposed kinetic model requires a vacant surface site, is poisoned more severely by oxygen than H_2CO formation at high P_{O_2}. Therefore a weakening in the metal–oxygen bond accelerates CO_2 formation more quickly than H_2CO formation.

In order to explain the observed very pronounced increase in both reaction rates with negative currents one must take into account that decreasing catalyst work function causes an increase in the metal–electron acceptor adsorbate bond strengths. This has been shown already in the case of CH_3OH dehydrogenation and decomposition on Ag (*27*) to drastically promote both the dehydrogenation and the decomposition rates. This is because an increase in the metal–electron acceptor adsorbate bond strength is expected from classical bond-order and bond-energy conservation considerations to cause a weakening in the intraadsorbate bonds and a concomitant increase in the rates of dehydrogenation and decomposition:

$$CH_3OH \rightarrow H_2CO + H_2 \qquad (35)$$

$$CH_3OH \rightarrow CO + 2H_2 \qquad (36)$$

Carbon monoxide is rapidly oxidized to CO_2 by chemisorbed oxygen, thus the rate of CO_2 formation is also accelerated. More negative potentials favor further abstraction of hydrogen from methanol and formaldehyde to form CO and, therefore, the selectivity to CO_2 increases as experimentally observed.

It is also likely that very negative potentials activate the CO disproportionation

route with a concomitant cleavage of the C–O bond (*24*), thus also activating the latent secondary pathway observed by McCabe (*35*) for CO_2 production from methanol.

The above considerations provide a qualitative explanation for all the observed aspects of the NEMCA behaviour of this catalytic system. Due to the complexity of the system it is not possible to make the discussion more quantitative as, for example, in the case of C_2H_4 oxidation on Pt (*26*), where the reaction mechanism is much more studied and understood. However, despite the complexity of the open-circuit kinetics of this reaction system, its NEMCA behaviour is described again by rather simple equations which show that, in general, catalytic rates depend exponentially on catalyst work function. This is the general conclusion of all studies of the NEMCA effect (*25–31*), including the present results.

From a practical viewpoint it is somehow disappointing that the maximum observed selectivity to H_2CO does not differ significantly from the regular catalytic value, since the maximum occurs very near the open-circuit conditions. However, there is no reason to expect that this will turn out to be a general observation in NEMCA studies of partial oxidation reactions.

CONCLUSIONS

The rate and selectivity of the Pt catalyzed methanol oxidation can be altered dramatically by controlling the catalyst surface work function independently from the gas phase via the NEMCA effect. The increases in catalytic rates are 10^3–10^4 times higher than the rate of O^{2-} transport to or from the catalyst and exceed the regular open-circuit catalytic rates by up to a factor of 15. Over wide ranges of experimental conditions catalytic rates depend exponentially on catalyst potential as in previous studies of the NEMCA effect (*24–29*). In view of the recent Kelvin probe-aided experimental validation (*32*) of the theoretically proposed (*26, 27*) equation $e\Delta V_{WR} = \Delta e\Phi$, where $\Delta e\Phi$ is the change in catalyst surface work function (*32*), it follows that over wide ranges of experimental conditions catalytic rates depend exponentially on catalyst surface work function. The use of TPD to study the state of adsorbed species on metal surfaces subject to O^{2-} pumping appears to be the next logical step for a further elucidation of the NEMCA effect, which is of considerable theoretical and practical importance.

ACKNOWLEDGMENTS

Financial support from the VW Stiftung of the Federal Republic of Germany and from the European Economic Community Nonnuclear Energy Program is gratefully acknowledged. We also thank one of our reviewers for some very useful comments.

REFERENCES

1. Vayenas, C. G., *Solid State Ionics* **28–30,** 1521 (1988).
2. Lintz, H.-G., and Vayenas, C. G., *Angew. Chem.* **101**(6), 729 (1989); *Int. Ed. Engl.* **28**(6), 708 (1989).
3. Stoukides, M., *Ind. Eng. Chem. Res.* **27,** 1745 (1988).
4. Gellings, P. J., Koopmans, H. J. A., and Burgraaf, A. J., *Appl. Catal.* **39,** 1 (1988).
5. Vayenas, C. G., and Satsburg, H., *J. Catal.* **57,** 296 (1979).
6. Stoukides, M., and Vayenas, C. G., *J. Catal.* **64,** 18 (1980).
7. Stoukides, M., and Vayenas, C. G., *J. Catal.* **69,** 18 (1981).
8. Stoukides, M., and Vayenas, C. G., *J. Catal.* **82,** 45 (1983).
9. Häfele, E., and Lintz, H.-G., *Ber. Bunsenges. Phys. Chem.* **92,** 188 (1988).
10. Vayenas, C. G., Lee, B., and Michaels, J. N., *J. Catal.* **66,** 36 (1980).
11. Vayenas, C. G., Georgakis, C., Michaels, J. N., and Tormo, J. *J. Catal.* **67,** 348 (1981).
12. Häfele, E., and Lintz, H.-G., *Ber. Busenges. Phys. Chem.* **90,** 298 (1986).
13. Yentekakis, I. V., Neophytides, S., and Vayenas, C. G., *J. Catal.* **111,** 152 (1988).
14. Pancharatnam, S., Huggins, R. A., and Mason, D. M., *J. Electrochem. Soc.* **122,** 869 (1975).
15. Gür, T. M., and Huggins, R. A., *J. Electrochem. Soc.* **126,** 1067 (1979).
16. Gür, T. M., and Huggins, R. A., *Science* **219,** 967 (1983).
17. Gür, T. M., and Huggins, R. A., *J. Catal.* **102,** 443 (1986).
18. Otsuka, K., Yokoyama, S., and Morikawa, A., *Chem. Lett. Chem. Soc. Japan* 319 (1985).
19. Seimanides, S., and Stoukides, M., *J. Electrochem. Soc.* **133,** 1535 (1986).

20. Hayakawa, T., Tsunoda, T., Orita, H., Kameyama, T., Takahashi, H., Takehira, K., and Fukuda, K., *J. Chem. Soc. Japan Chem. Commun.* 961 (1986).
21. Stoukides, M., and Vayenas, C. G., *J. Catal.* **70,** 137 (1981).
22. Stoukides, M., and Vayenas, C. G., *ACS Symp. Ser.* **178,** 182 (1981).
23. Stoukides, M., and Vayenas, C. G., *J. Electrochem. Soc.* **131,** 839 (1984).
24. Yentekakis, I. V., and Vayenas, C. G., *J. Catal.* **111,** 170 (1988).
25. Vayenas, C. G., Bebelis, S., and Neophytides, S., *J. Phys. Chem.* **92,** 5083 (1988).
26. Bebelis, S., and Vayenas, C. G., *J. Catal.* **118,** 125 (1989).
27. Neophytides, S., and Vayenas, C. G., *J. Catal.* **118,** 147 (1989).
28. Vayenas, C. G., Bebelis, S., Neophytides, S., and Yentekakis, I. V., *Appl. Phys. A.* **49,** 95 (1989).
29. Vayenas, C. G., Bebelis, S., and Neophytides, S., *in* "New Developments in Selective Oxidation" (G. Centi and P. Trifiro, Eds.), Studies in Surface Science and Catalysis, Vol. 55, pp. 643–652. Elsevier, Amsterdam, 1990.
30. Vayenas, C. G., Bebelis, S., Yentekakis, I. V., Tsiakaras, P., and Karasali, H., *Platinum Met. Rev.*, **34,** 122 (1990).
31. Vayenas, C. G., Bebelis, S., and Despotopoulou, M., *J. Catal.*, in press (1991).
32. Vayenas, C. G., Bebelis, S., and Ladas, S., *Nature (London)* **343,** 625 (1990).
33. Firth, J. G., *J. Chem. Soc. Faraday Trans. I* **67,** 212 (1971).
34. Gentry, S. J., Jones, A., and Walch, P. T., *J. Chem. Soc. Faraday Trans. I* **76,** 2084 (1980).
35. McCabe, R. W., and McCready, D. F., *J. Phys. Chem.* **90,** 1428 (1986).
36. Abbas, N. M., and Madix, R. J., *Appl. Surf. Sci.* **7,** 241 (1981).
37. Sexton, B. A., *Surf. Sci.* **102,** 271 (1981).
38. Wang, D. Y., and Nowick, A. S., *J. Electrochem. Soc.* **126,** 1155 (1979).
39. Bard, A. J., and Faulkner, L. R., "Electrochemical Methods: Fundamentals and Applications," pp. 230–240, 569–571. Wiley, New York, 1980.
40. Manton, M., Sc.D. thesis, MIT, 1986.
41. Herring, C., and Nichols, M. H., *Rev. Mod. Phys.* **21,** 185 (1949).
42. Reiss, H., *J. Phys. Chem.* **89,** 3783 (1985).
43. Boudart, M., *J. Amer. Chem. Soc.* **74,** 3556 (1952).
44. Gundry, P. M., and Tompkins, F. C., *in* "Experimental Methods in Catalytic Research" (R. B. Anderson, Ed.), pp. 100–168. Academic Press, New York, 1968.
45. Shustorovich, E., *Surf. Sci. Rep.* **6,** 1 (1986).
46. Blyholder, G., *J. Phys. Chem.* **68,** 2772 (1964).
47. Yentekakis, I. V., Bebelis, S., and Vayenas, C. G., in preparation.